Measurement of mechanical tractions exerted by cells in three-dimensional matrices

Wesley R Legant[1], Jordan S Miller[1], Brandon L Blakely[1], Daniel M Cohen[1], Guy M Genin[2] & Christopher S Chen[1]

Quantitative measurements of cell-generated forces have heretofore required that cells be cultured on two-dimensional substrates. We describe a technique to quantitatively measure three-dimensional traction forces exerted by cells fully encapsulated in well-defined elastic hydrogel matrices. Using this approach we measured traction forces for several cell types in various contexts and revealed patterns of force generation attributable to morphologically distinct regions of cells as they extend into the surrounding matrix.

Cells are constantly probing, pushing and pulling on the surrounding extracellular matrix. These cell-generated forces drive cell migration and tissue morphogenesis, and maintain the intrinsic mechanical tone of tissues[1,2]. Such forces not only guide mechanical and structural events but also trigger signaling pathways that promote functions ranging from proliferation to stem-cell differentiation[3,4]. Therefore, precise measurements of the spatial and temporal nature of these forces are essential to understanding when and where mechanical events come to play in both physiological and pathological settings.

Methods using planar elastic surfaces or arrays of flexible cantilevers have been used to map, with subcellular resolution, the forces that cells generate against their substrates[1,5–7]. But many processes are altered when cells are removed from native three-dimensional (3D) environments and maintained on two-dimensional (2D) substrates. Cells encapsulated in a 3D matrix exhibit dramatically different morphology, cytoskeletal organization and focal adhesion structure from those on 2D substrates[8]. Even the initial means by which cells attach to and spread against a 2D substrate are quite different from the invasive process required for cells to extend inside a 3D matrix. These

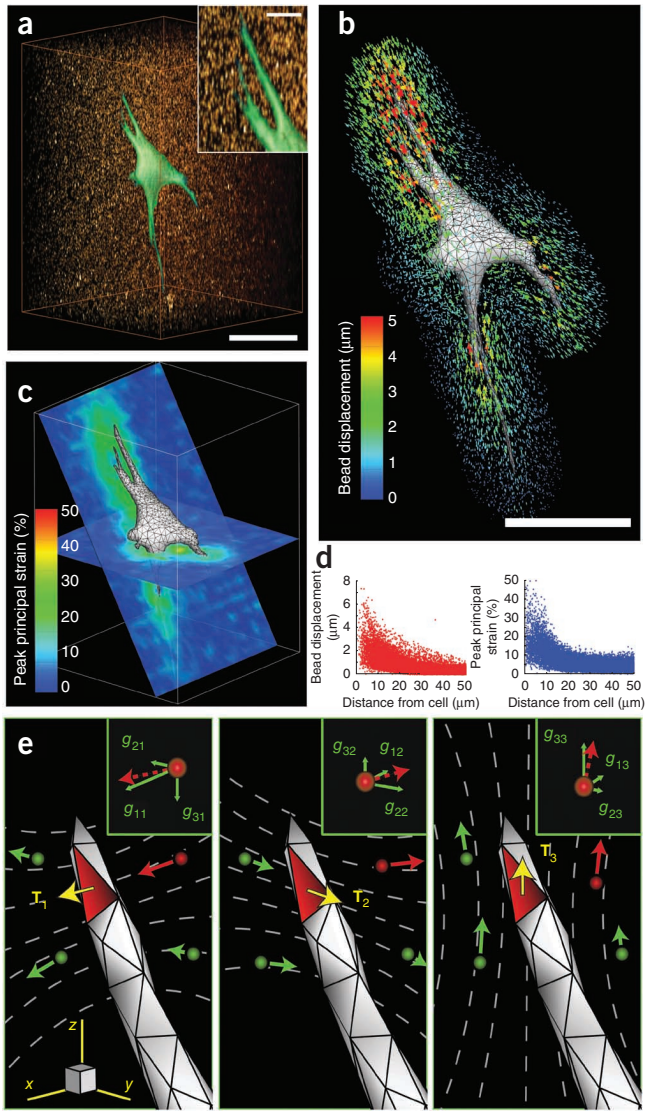

Figure 1 | Cell-induced hydrogel deformations and construction of a discretized Green's function. (**a**) Volume rendering of an EGFP-expressing NIH 3T3 fibroblast spreading into a 3D hydrogel containing fluorescent beads (red). Scale bar, 50 μm (10 μm in inset). (**b**) Bead displacement trajectories color coded by magnitude. Scale bar, 50 μm. (**c**) Two-dimensional slices through the volume showing the magnitude of the peak principal strain in the hydrogel surrounding the cell. (**d**) Plots of bead displacements and hydrogel strain as a function of distance from the cell surface. (**e**) Schematic outlining the use of the finite element method to reconstruct the Green's function. Surface traction (**T**) applied to the highlighted facet induced displacements of the surrounding beads (g_{ij}, inset). When repeated over all facets and beads, these relationships describe a discretized Green's function that can be used to calculate the tractions applied by the cell. The subscript indices of **T** and *g* represent the Cartesian components of the bead displacement in direction *i* in response to an applied surface traction in direction *j*.

[1]Department of Bioengineering, University of Pennsylvania, Philadelphia, Pennsylvania, USA. [2]Department of Mechanical, Aerospace and Structural Engineering, Washington University in St. Louis, St. Louis, Missouri, USA. Correspondence should be addressed to C.S.C. (chrischen@seas.upenn.edu).

RECEIVED 7 JULY; ACCEPTED 19 OCTOBER; PUBLISHED ONLINE 14 NOVEMBER 2010; DOI:10.1038/NMETH.1531

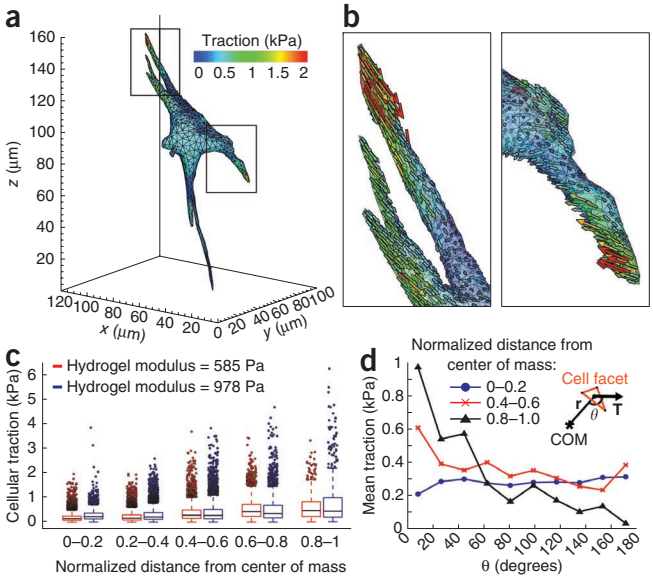

Figure 2 | Measurement of tractions exerted by live cells. (**a**) Contour plot of the tractions (magnitude) exerted by a cell. (**b**) Magnification of sections outlined in **a**, showing the individual traction vectors on each facet. (**c**) Boxplot of the traction magnitudes as a function of the normalized distance from the center of mass of the cell. This normalized distance was ~1 for the most spread regions (such as tips of long, slender extensions) and ~0 for the central cell body. (**d**) Mean traction at a given angle for cells encapsulated in 978 ± 228 Pa hydrogels. Inset, the angle (θ) was computed between the traction vector (**T**) and the position vector (**r**) of the cell facet with respect to the cell's center of mass (COM). Data shown in **c** and **d** are for 12 cells for each condition.

differences suggest that dimensionality alone may substantially impact how cellular forces are generated and transduced into biochemical or structural changes. Although the mechanical properties of 3D extracellular matrices and the cellular forces generated therein have been shown to regulate many cellular functions[9], to our knowledge, cellular forces in a 3D context have yet to be quantitatively measured.

Here we quantitatively measure the traction stresses (force per area), hereafter referred to as 'tractions', exerted by cells embedded in a hydrogel matrix. We encapsulated enhanced GFP (EGFP)-expressing fibroblasts in mechanically well-defined polyethylene glycol (PEG) hydrogels that incorporate proteolytically degradable domains in the polymer backbone and pendant adhesive ligands[10]. Incorporation of adhesive and degradable domains permitted the cells to invade, spread and adopt physiologically relevant morphologies (**Fig. 1a** and **Supplementary Movie 1**). The hydrogels used in this study had a Young's modulus of 600–1,000 Pa (**Supplementary Fig. 1**), a range similar to that of commonly used extracellular matrices such as reconstituted collagen or Matrigel and to *in vivo* tissues such as mammary and brain tissue[11,12]. Cells in 3D PEG gels deformed the surrounding matrix, which we visualized by tracking the displacements of 60,000–80,000 fluorescent beads in the vicinity of each cell (**Fig. 1b**, **Supplementary Fig. 2**, **Supplementary Note 1** and **Supplementary Movie 2**). We determined bead displacements relative to a reference stress-free state of the gel after lysing the cell with detergent (**Supplementary Movie 3**). Typically we observed deformations of 20–30% peak principal strain in much of the hydrogel surrounding the cell (**Fig. 1c**,**d**). The largest strains, up to 50%, occurred in the vicinity of long, slender extensions, which is consistent with observations of strong forces exerted by these regions on 2D substrates[13]. Because the mechanics of the PEG hydrogels showed no substantial dependence on strain or frequency (**Supplementary Fig. 1**), we used linear elasticity theory and the finite element method to determine the cellular tractions that would give rise to the measured bead displacements. Briefly, we generated a finite element mesh of the hydrogel surrounding the cell from confocal images. We constructed a discretized Green's function by applying unit tractions to each facet on the surface of the cell mesh and solving the finite element equations to calculate the induced bead displacements (**Fig. 1e**). Standard regularization methods for ill-posed, overdetermined linear systems of equations were then used to compute the tractions exerted by the cell (**Supplementary Note 2**). The time required to calculate a single dataset was ~4.5 h using readily available computational equipment. However, we could reduce this dramatically by using a simplified finite element mesh of the cell and hydrogel. These lower-resolution datasets still captured the fundamental character of higher-resolution measurements (**Supplementary Fig. 3**).

To validate the approach and to characterize its spatial resolution, we used simulated traction fields (**Supplementary Fig. 4**). We measured experimental noise owing to bead displacements in cell-free regions of the hydrogel before and after detergent treatment, and measured surface discretization noise from multiple discretizations of the same cells. Then we superimposed these datasets onto the displacements generated by simulated loadings before traction reconstruction. In this setting, the percentage of traction recovered was proportional to the magnitude and characteristic length of the simulated loadings (defined as the average period of spatial oscillation). For all cases, the presence of noise reduced recovery accuracy by ~20–30%. Despite these limitations, the recovered tractions still captured the essential periodic features of even the most spatially complex simulated loadings with characteristic lengths of spatial variation down to 10 μm.

We next calculated the tractions from live cells encapsulated in 3D hydrogels and found that cells exerted 100–5,000-Pa tractions, with strong forces located predominantly near the tips of long, slender extensions (**Fig. 2a**,**b** and **Supplementary Movie 4**). For all measurements, forces were in static equilibrium with a typical error of ~1–5% of the total force applied by the cell. Subsequent analysis revealed that these tractions were minimally impacted by possible variations in local hydrogel mechanics or by uncertainty in the measured bead displacements (**Supplementary Figs. 5** and **6**). Previous measurements of cellular forces on 2D surfaces have generally been limited to shear loadings, although recent studies have measured small forces exerted normal to the planar surface as well[14,15]. It is unclear, however, whether these relationships might be altered for cells inside a 3D matrix. Here we found that cells encapsulated in a 3D matrix predominantly exerted shear tractions, although small normal tractions were also present near the cell body. To determine whether patterns of force might be associated with specific cell regions, we quantified the magnitude and angle of tractions with respect to the center of mass of the cell. Generally, tractions increased as a function of distance from the center of mass (**Fig. 2c**). Cells encapsulated in hydrogels with a Young's modulus of ~1,000 Pa generated stronger tractions than those in ~600-Pa hydrogels. The observed differences in tractions were not due to an overall increase in total cellular contractility, as

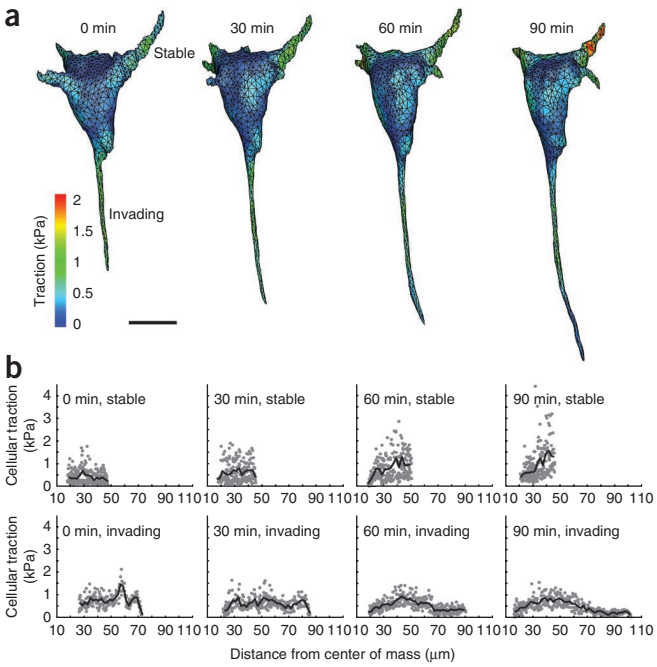

Figure 3 | Measurement of dynamic tractions exerted by spreading cells. (**a**) Contour plot of the tractions (magnitude) exerted by a cell as it invades into the surrounding hydrogel at indicated times relative to the beginning of measurement. Scale bar, 20 μm. (**b**) Tractions exerted by extensions labeled in **a** as a function of distance from the center of mass of the cell.

measured by the net contractile moment (**Supplementary Fig. 7**) but rather were most apparent in strong inward tractions near the tips of long, slender extensions (**Fig. 2c**). This reveals a local and nonlinear reinforcement of cellular contractility in response to substrate rigidity and suggests that such regions may be hubs for force-mediated mechanotransduction in 3D settings. The cell bodies showed no bias in traction angle, but strong tractions became progressively aligned back toward the center of mass in more well-spread regions of the cell (for example, near the tips of long, slender extensions) (**Fig. 2d**). In general, these patterns of force were reflected in multiple cell types but could be altered by cell-cell proximity or maintenance as a multicellular aggregate. Neighboring NIH 3T3 cells preferentially extended away from each other, whereas proliferating multicellular tumor spheroids exerted outward normal tractions on the matrix (**Supplementary Figs. 8** and **9**).

Upon closer inspection we found a subset of extensions that displayed strong tractions several micrometers behind the leading tip, whereas the tractions at the tip itself were substantially lower. As such traction profiles are similar to those observed behind the leading edge of a lamellipodia for a migrating cell on a 2D substrate[1], we hypothesized that such regions may represent invading or growing cellular extensions in three dimensions. To test this possibility, we measured the tractions from time-lapse images of cells as they invaded the surrounding hydrogel (**Fig. 3a**). Indeed, tractions at the tips of growing extensions were notably lower than the strong tractions exerted by proximal regions of the same extension (**Fig. 3b** and **Supplementary Fig. 10**). However, we did not observe normal forces pushing into the extracellular matrix in these extensions, which suggests that a local inhibition of myosin-generated contractility allows tip advancement. Moreover, we also detected strong tractions from small extensions on the cell face opposite the invading extensions. Such stable extensions exhibited very different force distributions than the growing extensions, often lacking the characteristic drop in force near the leading edge, and may correspond to an anterior-posterior polarity axis formed in the cell.

These data suggest that cells in 3D matrices probe the surrounding extracellular matrix primarily through strong inward tractions near the tips of long, slender extensions. This technique was generalizable to different cell types, cell-cell interactions and even to multicellular tumor structures in which both tumor growth and invasion have been previously shown to be mechanoresponsive[11]. Because the synthetic hydrogels used in this study had similar elastic moduli to *in vivo* tissues[11,12] and can support many cellular functions[16], we anticipate that this approach will enable investigations into the role of cellular forces in various biological settings.

METHODS

Methods and any associated references are available in the online version of the paper at http://www.nature.com/naturemethods/.

Note: Supplementary information is available on the Nature Methods website.

ACKNOWLEDGMENTS

We thank J. Baranski, H. Hu, C. Shen and M. Wozniak for helpful discussions. This work was supported in part by grants from the US National Institutes of Health (EB00262, EB08396, GM74048, HL73305 and HL90747), the Resbio Technology Resource for Polymeric Biomaterials, the Material Research Science and Engineering Center and Center for Engineering Cells and Regeneration at the University of Pennsylvania, the National Science Foundation graduate research fellowship (W.R.L. and B.L.B.), the US National Institutes of Health T32 training grant and the Hartwell Foundation (J.S.M.).

AUTHOR CONTRIBUTIONS

W.R.L., G.M.G. and C.S.C. conceived and initiated the project. W.R.L., J.S.M., B.L.B. and D.M.C. designed and performed experiments. C.S.C. supervised the project.

COMPETING FINANCIAL INTERESTS

The authors declare no competing financial interests.

Published online at http://www.nature.com/naturemethods/.
Reprints and permissions information is available online at http://npg.nature.com/reprintsandpermissions/.

1. Dembo, M. & Wang, Y.L. *Biophys. J.* **76**, 2307–2316 (1999).
2. Keller, R., Davidson, L.A. & Shook, D.R. *Differentiation* **71**, 171–205 (2003).
3. Huang, S., Chen, C.S. & Ingber, D.E. *Mol. Biol. Cell* **9**, 3179–3193 (1998).
4. McBeath, R., Pirone, D.M., Nelson, C.M., Bhadriraju, K. & Chen, C.S. *Dev. Cell* **6**, 483–495 (2004).
5. Balaban, N.Q. *et al. Nat. Cell Biol.* **3**, 466–472 (2001).
6. Butler, J.P., Tolic-Norrelykke, I.M., Fabry, B. & Fredberg, J.J. *Am. J. Physiol. Cell Physiol.* **282**, C595–C605 (2002).
7. Tan, J.L. *et al. Proc. Natl. Acad. Sci. USA* **100**, 1484–1489 (2003).
8. Cukierman, E., Pankov, R., Stevens, D.R. & Yamada, K.M. *Science* **294**, 1708–1712 (2001).
9. Pampaloni, F., Reynaud, E.G. & Stelzer, E.H. *Nat. Rev. Mol. Cell Biol.* **8**, 839–845 (2007).
10. Miller, J.S. *et al. Biomaterials* **31**, 3736–3743 (2010).
11. Paszek, M.J. *et al. Cancer Cell* **8**, 241–254 (2005).
12. Discher, D.E., Janmey, P. & Wang, Y.L. *Science* **310**, 1139–1143 (2005).
13. Chan, C.E. & Odde, D.J. *Science* **322**, 1687–1691 (2008).
14. Maskarinec, S.A., Franck, C., Tirrell, D.A. & Ravichandran, G. *Proc. Natl. Acad. Sci. USA* **106**, 22108–22113 (2009).
15. Hur, S.S., Zhao, Y., Li, Y.S., Botvinick, E. & Chien, S. *Cell. Mol Bioeng.* **2**, 425–436 (2009).
16. Lutolf, M.P. & Hubbell, J.A. *Nat. Biotechnol.* **23**, 47–55 (2005).